Journal of Physics: Theories and Applications E-ISSN: 2549-7324 / P-ISSN: 2549-7316
J. Phys.: Theor. Appl. Vol. 9 No. 1 (2025) 37-51 doi: 10.20961/jphystheor-appl.v9i1.99996

Optimizing high-order harmonic generation with two-color fields, polarization gating, and static electric fields

Onsure Duke Nyangau[1]., Kebwaro Jeremiah Monari[1], Rurimo Kihara[2] & Njoroge Stephen Maina[1†]

[1]Department of Physical and Biological Sciences Karatina University, P.O. Box 1957-10101, Karatina, Kenya

[2]National Institute of Optics and Laser, Multimedia University of Kenya, P.O. Box 15653-00503, Nairobi, Kenya

[†]Corresponding author: snjoroge@karu.ac.ke

Received 18 January 2025, Revised 3 March 2025, Published 31 March 2025

Abstract: The optimization of high order harmonic generation process under the combination of a plasmonic enhanced two color field with modulated polarization gating and a static electric field was investigated in this study. Through investigating the harmonic spectrum yields by numerical solution of the one-dimensional time dependent Schrödinger equation, it is shown that the inhomogeneity of the local fields, polarization angle, confinement of the electron movement through the use of two color and static electric fields plays an important role in the HHG process. It is further observed that when the three schemes are used together a high harmonic yield, broadened harmonic plateau and a significantly increased harmonic cutoff point up to 600^{th} order are obtained confirming an improved harmonic conversion efficiency.

Keywords: High-order harmonic generation, attosecond pulses, harmonic spectrum, harmonic conversion efficiency, lasers

1. Introduction

High-order harmonic generation (HHG) is a nonlinear process that involves the interaction of an intensely focused laser field with matter Park *et al*. (2021), Neufeld *et al*. (2022), Gao *et al*. (2022) and Ganeev (2022) resulting to the emission of coherent light at frequencies that are integer multiples (harmonics) of the original laser frequency (Gao *et al*., 2022, Ganeev, 2022 and Boltaev *et al*., 2021). In the recent years, HHG has been intensively researched both in theory Yue *et al*. (2022), Li *et al*. (2021), Yue & Gaarde (2021) and Kanega *et al*. (2021) as well as in experiment Chevreuil *et al*. (2021), Iqbal *et al.* (2022), Davino *et al*. (2021) and Ren *et al*. (2024) because it offers an effective technique to generate extreme ultraviolet (XUV) Boltaev *et al*. (2021) and Krausz & Ivanov (2009), soft X-rays Abbing *et al*. (2021) and Popmintchev *et al*. (2012) as well as attosecond pulses (Njoroge & Kinyua, 2024, Weissenbilder *et al*., 2022, Constant *et al*., 2025, Li *et al*., 2024 and Yu *et al*., 2021). Production of isolated attosecond pulses from HHG process has been gaining a lot of interest lately because of its potential application in attosecond spectroscopy Li *et al*. (2024), Yu *et al*. (2021) and Yu *et al*. (2023) as well as in the study of ultrafast processes within atoms Gao *et al*. (2022) and Ganeev (2022)

and molecules (Wang *et al.*, 2024, Xiaohong *et al*., 2023 and Ciappina *et al*., 2017). Despite the promising applications of the attosecond pulses, low harmonic conversion efficiency in HHG process has continued to be a major drawback.

Several techniques for controlling harmonic conversion efficiency in HHG process such as using plasmonic enhanced laser field Zhang *et al*. (2012), Burnett & Rae (1993), Kim *et al*. (2008) and Feng *et al*. (2013), polarization gating Njoroge *et al*. (2019) and Koushki *et al*. (2018) and static electric field Zhang *et al*. (2012), Koushki & Sarikhani, (2020) and Silaev *et al*. (2022) have been proposed. When using the plasmonic enhanced field scheme, the mobility of electrons can be controlled by employing two or more laser pulses of different wavelengths that can be combined to form a complicated electric field (Ren *et al*., 2017). This approach eliminates the need to use extra cavities to amplify the input pulse power Njoroge & Kinyua (2024) and Salmeh & Mohebbi (2023) while at the same time enhancing the local fields by more than 20 dB Yuan et al. (2017) thus making it possible to achieve HHG below the harmonic threshold intensity (10^{13}W/cm^2). This scheme has been described to relatively easy and affordable Feng *et al*. (2013) and Vincenti *et al*. (2014) leading to its application in different fields, such as the investigation of ultrafast chemical reactions Gao *et al*. (2022), Ganeev (2022) and Bionta *et al*. (2021) and the production of high-order harmonics (Vincenti *et al*., 2014).

The addition of a static electric field has also been used as a technique in controlling harmonic conversion efficiency in HHG process. Studies have shown that the application of a static electric field along the laser polarization axis suppresses the transverse spreading of the electron wave packet (Zhang *et al*., 2012, Koushki & Sarikhani, 2020, Silaev *et al*., 2022 and Wang *et al*., 1999). One of the studies on HHG study from a helium ion model in a two-color laser field generated by a fundamental pulse and its second harmonic pulse produced a super-continuum spectrum in the two-color field whose spectral intensity was relatively low (Zhang *et al*., 2012). However, on adding a static electric field to the synthesized two-color field, there was a dramatic boost on the ionization yield of electrons contributing to harmonic emission, as well as the quantum pathways of the HHG and as a result, the extension and enhancement of the supercontinuum were achieved, producing a harmonic spectrum with a band width of about 170.5eV (Zhang *et al*., 2012). This study sought to theoretically investigate the control of HHG conversion efficiency by simultaneously employing three schemes; a plasmonic enhanced two-color field (synthesized by an 800nm fundamental pulse and a 1600nm control pulse), modulated polarization gating and a static electric field. Based on the results obtained by solving the one-dimensional time dependent Schrödinger equation (1D-TDSE), the study shows that HHG conversion efficiency is improved to a harmonic cutoff point of 600th harmonic order. The study further discusses the influence of the inhomogeneity parameters, relative angle of the two pulses and the static electric filed on the HHG conversion efficiency.

2. Theoretical model

The study was conducted through a simulation process. In the simulation, the harmonic spectra were generated by solving 1D-TDSE, expressed as follows;

$$\left[i\frac{\partial\Psi(x,t)}{\partial t} = H(x,t)\Psi(x,t)\right] \quad (1)$$

$$= \left[-\frac{1}{2}\frac{\partial^2}{\partial x^2} + V_a(x) + V_i(x,t)\right]\Psi(x,t) \quad (2)$$

Where $V_a(x) = -\frac{1}{\sqrt{x^2+\alpha}}$ is a soft-core potential and $V_l(x,t) = -E_x(x,t)x$ is the potential due to electron interaction. The soft core parameter α was chosen to be 0.1195 to match the ground ionization potential of neon atom which is 0.7925 a.u (21.6 eV). The x component of the inhomogeneous field was given by:

$$E_x(x,t) = E_x(t)\big(1+\varepsilon_x(x)\big) \quad (3)$$

Here the parameter ε_x defined the strength inhomogeneity of the laser field along the x direction (Pérez-Hernández et al., 2013)..

An 800-nm fundamental pulse and a 1600-nm control pulse with crossed linear polarizations were optimized and adopted to synthesize the two-color field. The intensities of these two laser pulses were optimized at 4.0 x 10^{14} Wcm^{-2} and 3.6 x $10^{14}Wcm^{-2}$ respectively. The electric field of the x component of the two-color field was given as:

$$E(t) = (\beta E_o + E_o[f_1(t)\cos\big(\omega_o t+\varphi(t)\big) + f_2(t)\cos\big(2\omega_o t+\varphi(t)\big)]e_x \quad (4)$$

Here β = the ratio of the static and the laser field, E_o = the amplitude of laser field, f_1 (t) and f_2 (t) represent the pulse envelopes.

The study used the split-operator method Feit et al. (1982) to solve equation 1. To avoid incorrect reflections from the boundaries, the electron wave-function is multiplied by a mask function at each time step (Krause et al., 1992). The neon atom is in the initial (ground) state before the laser is turned on. The ground state is obtained by imaginary time propagation with the soft-core potential. Once the electron wave function ψ (x, t) is obtained, the time-dependent dipole acceleration along x direction is calculated by the Ehrenfest theorem (Burnett & Rae, 1993)

$$a_x(t) = -\langle\varphi(x,t)\big|\big[H(x,t),[H(x,t),x]\big]\big|\varphi(x,t)\rangle \quad (5)$$

The HHG spectrum is obtained by Fourier transforming time-dependent dipole acceleration given as;

$$\left|S_{qx}(\omega)\right|^2 = \left|\frac{1}{T}\int_0^T a_x(t)e^{-iq\omega t}dt\right|^2 \quad (6)$$

Time-frequency analysis by means of wavelet transform (WT) is used to analyze the numerically generated HHG spectrum (Koushki *et al*., 2018). The equation is given as;

$$A(t,\omega) = \int d_a(t)\sqrt{\omega}W[\omega(t'-t)]dt' \quad (7)$$

Where d_a is the time dependent dipole acceleration and $W[\omega(t'-t)]$ is the mother wavelet. A natural choice of the mother wavelet is given by the mother Morlet wavelet;

$$\omega W[\omega(t'-t)] = \frac{1}{\sqrt{\pi^{\frac{1}{2}}\sigma}}\exp\left(i\omega(t'-t)\exp\left(\frac{-\omega^2(t'-t)^2}{2\sigma^2}\right)\right. \quad (8)$$

σ is the Gaussian width which will be set to be σ=2π

3. Results and Discussion

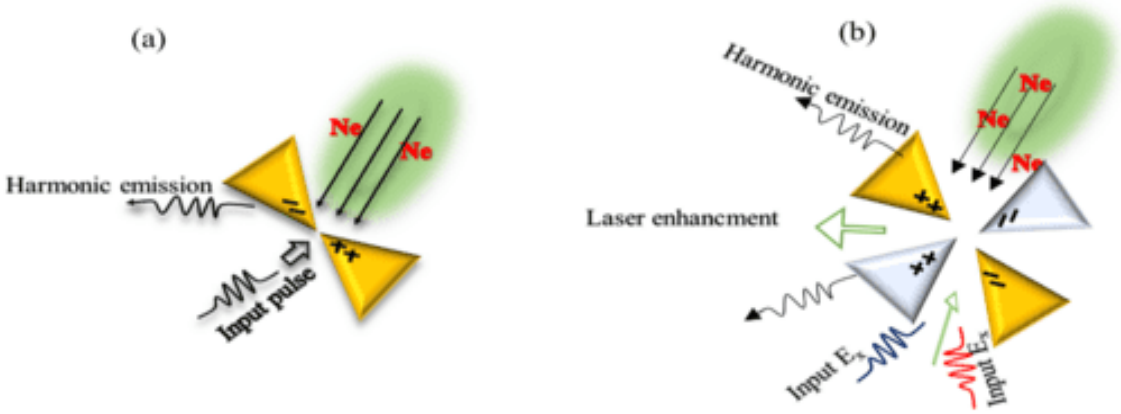

Figure 1. (a) Representation of electric field enhancement and harmonic emission using a nanostructure of bow-tie elements (b) the similar representation as that in Figure 1(a) but for two color field. Source: (Feng et al., 2013)

Plasmonic field enhancement is a technique used to generate high order harmonics by utilizing the local field improvement brought about by resonant plasmons in a metallic nanostructure made of bow-tie-shaped gold elements on a sapphire substrate Kim *et al*. (2008), whereby for a linear polarization, low intensity input laser pulse couples to the plasmon mode as shown in Figure 1(a). This results to a collective oscillation of the free charges around the vicinity of the metal nanostructure leading to the distribution of the negative charges around one apex and the positive charges around the other one. Consequently, by introducing neon gas into this improved field, an enhanced or extended HHG is realized (Feng et al., 2013). In the situation where the input pulse is chosen to be the two-color pulse with a good polarization phase as shown in Figure 1 (b) and also adopted in this study, the harmonic yield will be increased as well as harmonic modulation being reduced, leading to increased harmonic conversion efficiency.

The results in Figure 2(a) show the component of the generated harmonic spectrum in the homogeneous two-color field for different control laser field wavelengths while Figure 2 (b)-(d) shows the results of the corresponding time frequency distributions for the generated harmonic spectrum in Figure 1(a). Here, the fundamental field wavelength and its field intensity are chosen to be 800nm and $4.0 \times 10^{14} \mathrm{Wcm}^{-2}$ respectively while the inhomogeneity parameter, the relative phase angle and the static electric field are all set to zero.

As shown in Figure 2(a), when the control field's wavelength value is increased from 1400nm to 1800nm, not only do double harmonic plateaus form but also the harmonic cutoff point is extended to 240^{th} order. However the harmonic yield decreases progressively (from -2.8 to -3.5 arb. units) but with the most broadened harmonic spectrum upto 180 orders. The 1400nm field has its harmonic yield being the highest (-2.8 arb. units) compared to the 1600nm and 1800nm fields, however, the band width for the 1400nm is the shortest with 85 orders.

The 1800nm field has the largest band width (180 orders) but with the lowest harmonic yield (-3.5 arb. units) characterized with a lot of interference. The 1600nm field on the other hand has a relatively higher harmonic yield (-3.0 arb. units) with a wider band width spectrum up to 125 orders and few interferences. This is confirmed by comparing

the harmonic peaks; P_1 in Figure 2 (b), P_2 in Figure 2(c) and P_3 in Figure 2(d) that represent the harmonic cutoff from where it is observed it is observed that the 1600nm pulse in figure 2(c) produces a high yield harmonic spectrum with few modulation structures (peak P_2), hence chosen as the optimal wavelength for this study.

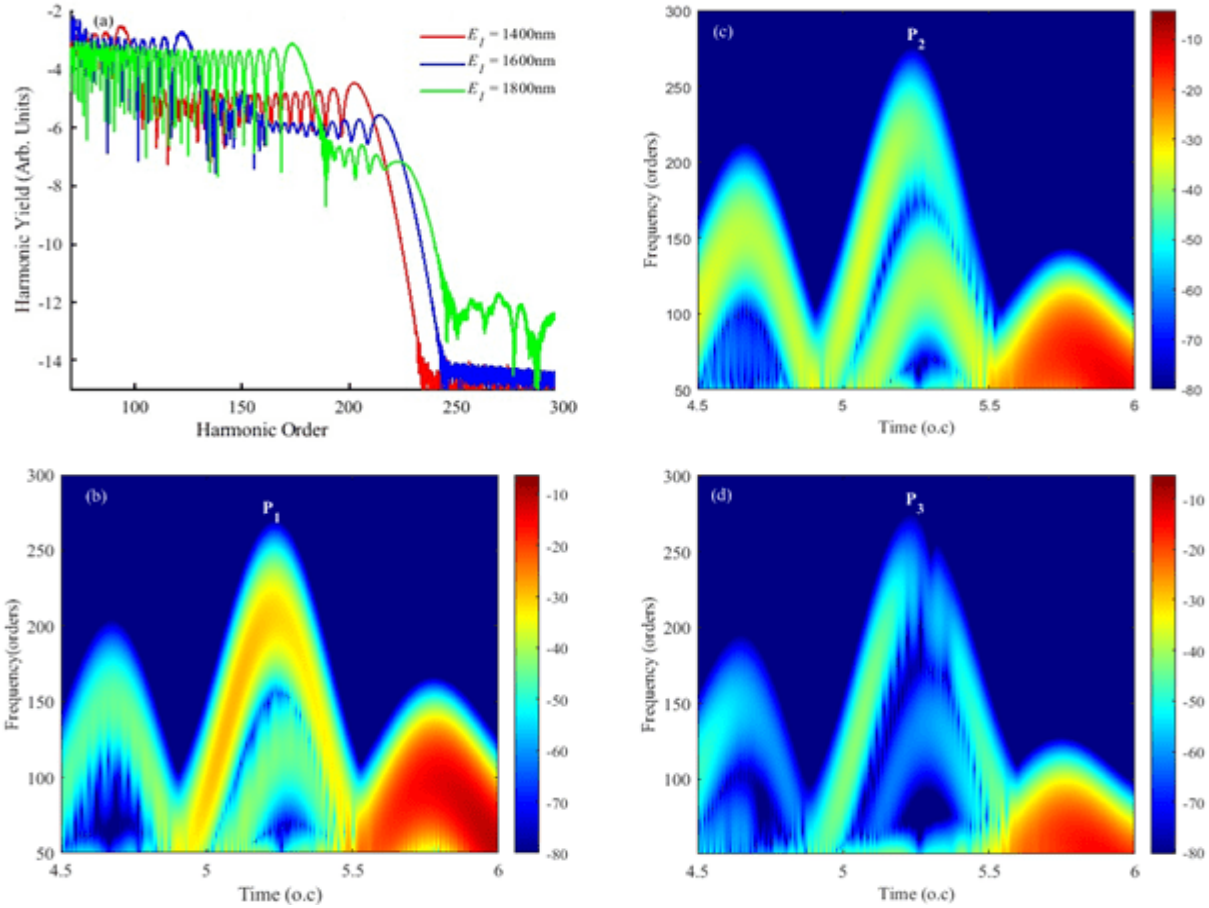

Figure 2. (a) the components of the generated harmonic spectrum in the homogeneous two-color field for different control pulse wavelength and (b)-(d) the corresponding time frequency distributions for the generated harmonic spectrum.

The results in Figure 3(a) show the component of the generated harmonic spectrum in the homogeneous two-color field for different polarization angles (θ) while Figures 3 (b), (c) and (d) show the corresponding time frequency distributions for the generated harmonic spectrum in Figure 3(a). Here, the other parameters are the same as the ones used in Figure 2. From figure 3(a), it can be clearly seen that as the polarization angle is increased, there is a significant broadening of the first and the second harmonic plateaus. At $\theta=0.1\pi$ the harmonic yield is high (-2.7 arb. units) with reduced modulation structures in the second plateau and an extended harmonic cutoff point (220^{th} order) is realized. The 0.3π polarization angle also gives a high harmonic yield (-3.0 arb units) but with increased modulation structures in the second plateau.

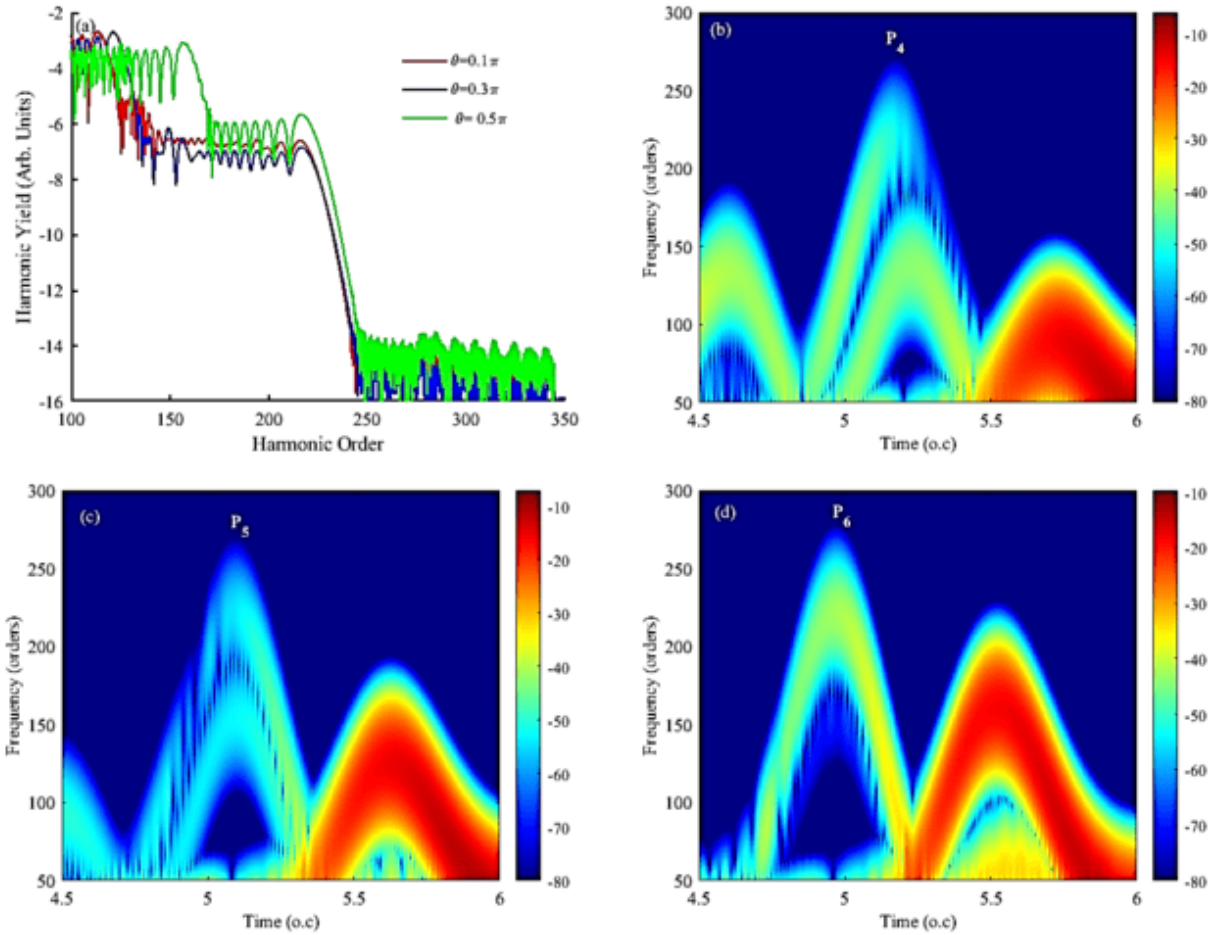

Figure 3. (a) The component of the generated harmonic spectrum in the homogeneous two-color field for different polarization angles and (b)-(d) the corresponding time frequency distributions for the generated harmonic spectrum.

The 0.5π polarization angle yields the lowest harmonic results (-3.6 arb. units) but with a broader but highly modulated harmonic spectrum. This is confirmed by comparing the time frequency distributions for the generated harmonic spectrum shown in form harmonic peaks; P_4, in Figure 3(b), P_5 in Figure 3(c) and P_6 in Figure 3(d). Figure 3(b) with peak P_4 shows that the harmonics above 200th order are continuous and can support a favorite attosecond pulse.

The results in Figure 4(a) show the components of the generated harmonic spectrum in the homogeneous two-color field for different intensities of the control pulse, while the corresponding time frequency distributions for the generated harmonic spectrum are shown in Figure 4(b) for 1.8 x 10^{14} Wcm^{-2}, (c), 3.6 x 10^{14} Wcm^{-2} and (d) 7.2 x 10^{14} Wcm^{-2}. Here, the inhomogeneity parameter and the static electric field are all set to zero while all other parameters are the same as the ones used in Figure 3.

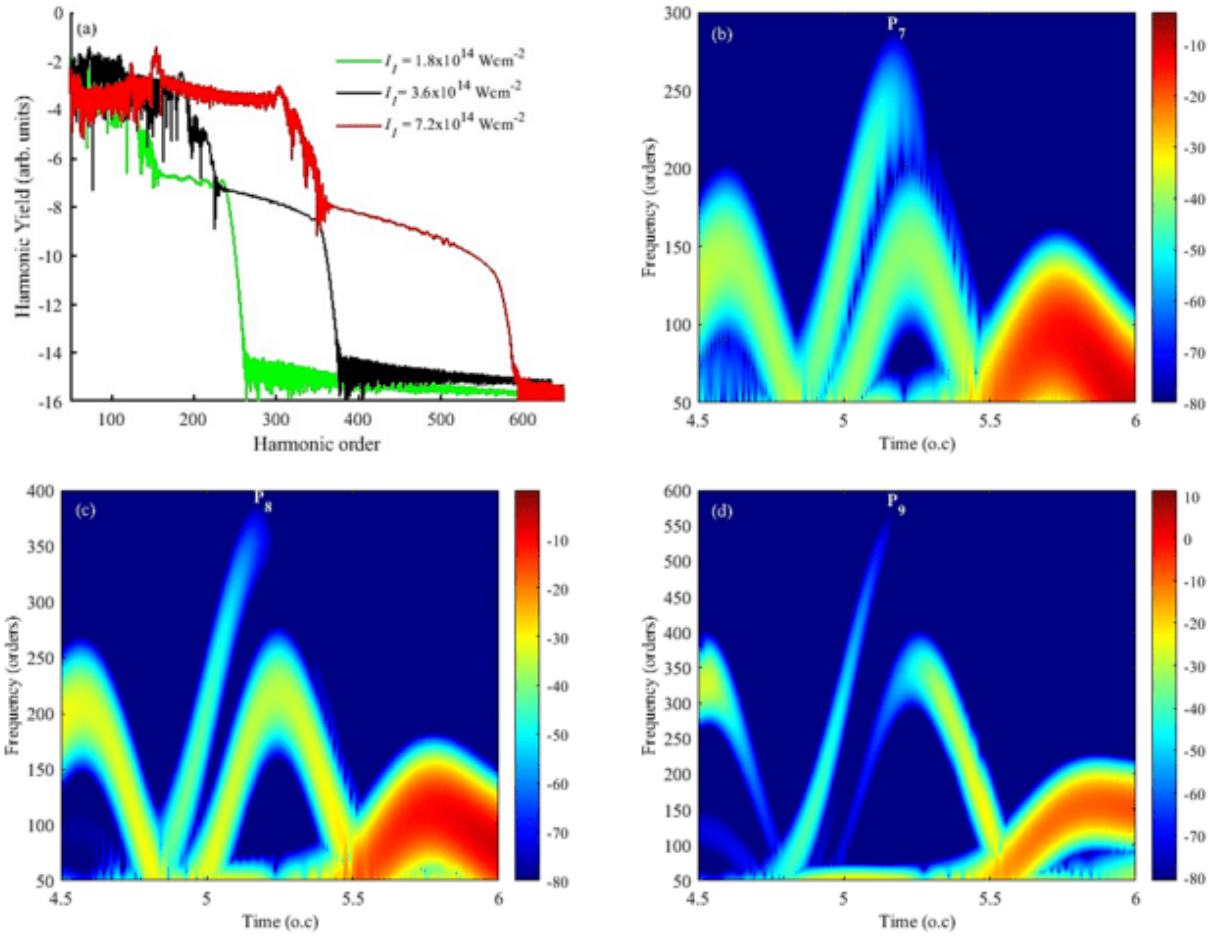

Figure 4. (a) the component of the generated harmonic spectrum in the homogeneous two-color field for different control pulse intensities and (b)-(d) the corresponding time frequency distributions for the generated harmonic spectrum.

As it can be seen from Figure 4(a), when the control field's intensity is varied from 1.8 x 10^{14} Wcm^{-2} to 7.2 x 10^{14}Wcm^{-2}, the second harmonic plateaus for each value broadens significantly as well as an extension of the harmonic cutoff point is realized compared to the results obtained in Figure 3. A two-color field with a properly adjusted wavelength and intensity yields better harmonic results compared to a single-color field since in the two-color field, there is an increase in the photon flux which influences the electron mobility within the continuum leading to an increased harmonic conversion efficiency. The harmonic peak P_8 in Figure 4 (c) shows characteristics of the possibility of forming a double peak when other parameters such as static electric field are adjusted.

The results in Figure 5 (a) shows the component of the generated harmonic spectrum in the two-color field when varying the inhomogeneity parameter while Figures 5 (b), (c) and (d) show the corresponding time frequency distributions for the generated harmonic spectrum. Here, only the static electric field is set to zero while the other parameters are the same as those used in Figure 4 with optimized control pulse intensity chosen to be 3.6 x10^{14} Wcm^{-2}. As the values of the inhomogeneity parameters are increased from 0.001 to 0.002, the number of harmonic plateaus is noted to increase from two (for 0.001) to three (for 0.0015 and 0.002).

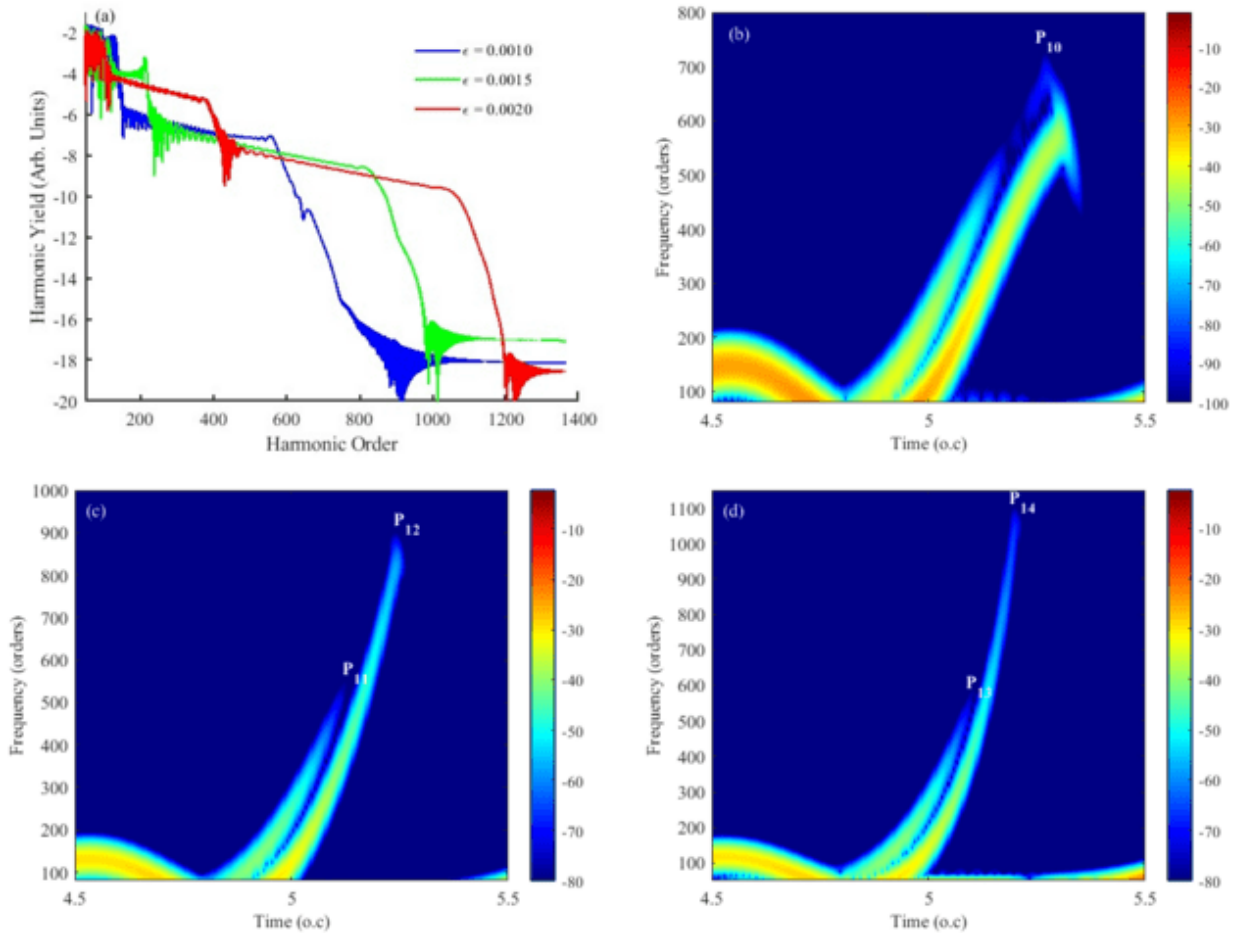

Figure 5. (a) The component of the generated harmonic spectrum in the inhomogeneous two-color field for different inhomogeneity parameters and (b)-(d) the corresponding time frequency distributions for the generated harmonic spectrum

The results in Figure 5 (b) corresponding to the 0.001 inhomogeneity parameter produced only one harmonic peak, P_{10} while the results in Figures 5 (c) and (d) corresponding to the inhomogeneity parameter of 0.0015 and 0.002 respectively, exhibited double harmonic peaks with their initial peaks (P_{11} and P_{13}) being significant in HHG process than their second peaks (P_{12} and P_{14}). The peaks are dissolved between 400-600 orders, representing two quantum paths (long and short electron trajectory paths). This lowers the harmonic conversion efficiency. The inhomogeneity parameter 0.001 is therefore chosen as the optimal value for the next experiment because of the broadened first plateau with few modulation structures.

The results in Figure 6(a) shows the component of the generated harmonic spectrum when using two-color fields for different static electric field values while Figures (b)-(d) show the corresponding time frequency distributions for the harmonic spectrum. Here, all other parameters are maintained as those used in Figure 5.

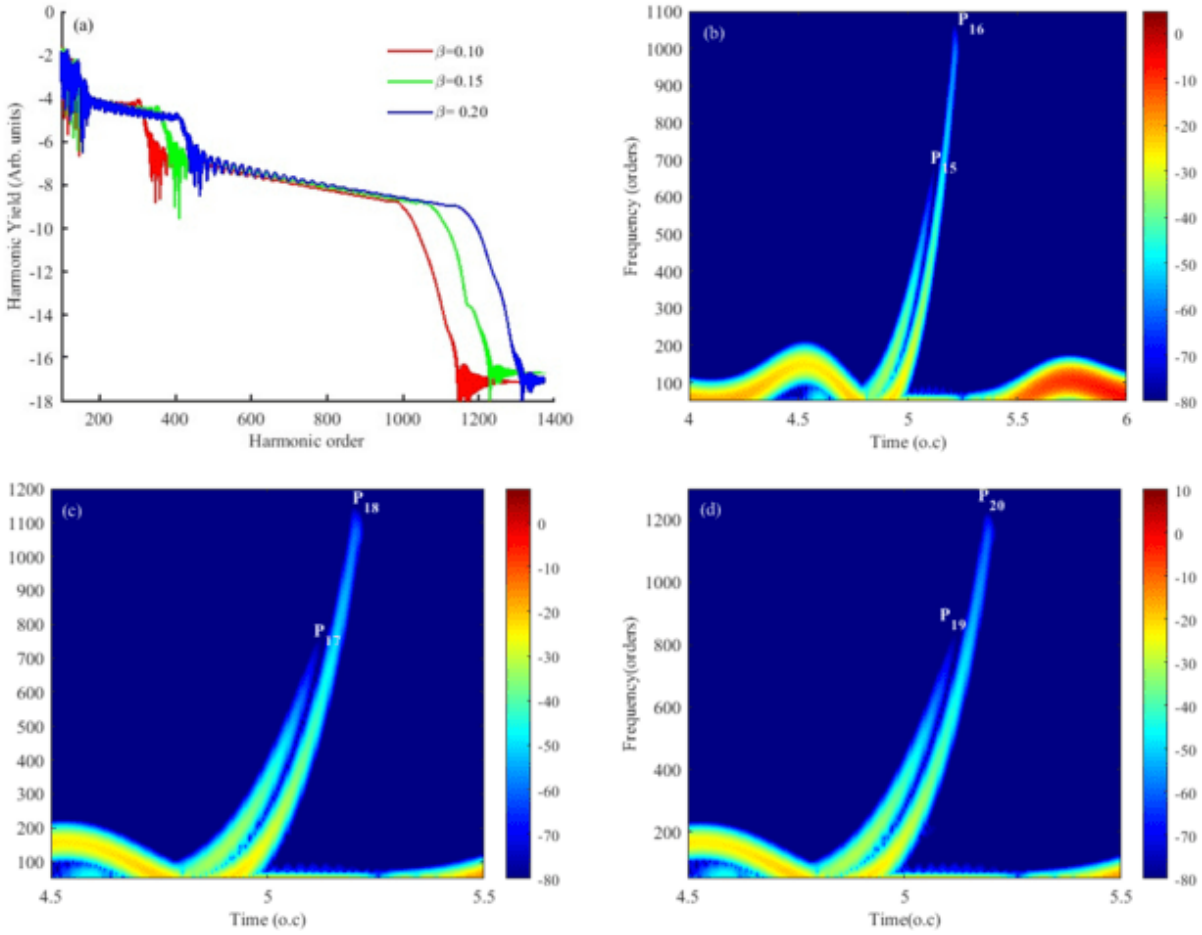

Figure 6. (a) The component of the generated harmonic spectrum in the inhomogeneous two-color field with static electric field and (b-d) the corresponding time frequency distributions for the generated harmonic spectrum.

The results in Figure 6 show a significant increase of the harmonic yield and broadening of the harmonic plateau as well as an extension of the harmonic cutoff point as the static electric field is increased. Static electric field of value 0.2 as shown in Figure 6(a) gives the highest harmonic yield with the most extended harmonic cutoff point but with a lot of modulation. Increasing static electric field causes more ionization which leads to increased quantum paths and return time, thus decreasing harmonic conversion efficiency. Figure 6(b) with harmonic peaks P_{15} and P_{16}, Figure 6(c) with harmonic peaks P_{17} and P_{18} and Figure 6(d) with harmonic peaks P_{19} and P_{20} show the respective cutoff points. Double peaks are formed in each case with the first peaks contributing significantly to HHG process. Peak P_{15} from the static electric value β=0.1 is chosen as the optimal value due to low interference.

The results in Figure 7 (a) show a comparison of various results when using homogeneous two-color field without static electric field and inhomogeneity parameter. Here, it is shown that before introducing the polarization angle and the intensity of the control field, the harmonic cutoff is at 220^{th} order. When the polarization angle is introduced and set at 0.1π, the harmonic cutoff point is maintained at the 220^{th} order but the harmonic yield increases as well as the smoothening of the plateau is observed.

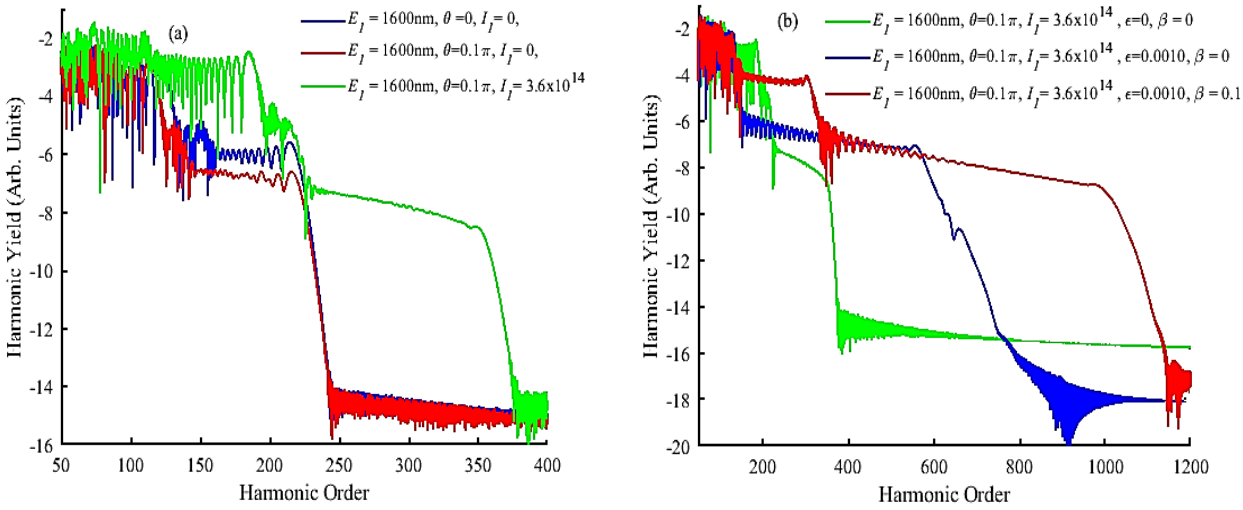

Figure 7 (a) comparison of the component of the generated harmonic spectrum for a two-color field without inhomogeneity parameters and static electric field (b) component of the generated harmonic spectrum with inhomogeneity parameters and static electric field

Further, when the intensity of the control filed is adjusted as shown using green line in Figure 7(a), a broader harmonic plateau and a higher harmonic yield are both achieved, showing an extension in the harmonic cutoff point to 360th order. Figure 7 (b) shows the generated harmonic spectrum comparing different results when using two color inhomogeneous field in the absence and presence of the static electric field. All other values used are same as those in Figure 7(a). It can be shown that with the introduction of the inhomogeneity parameters, the harmonic cutoff is remarkably enhanced as well as a reduction in harmonic modulation. Further, the addition of static electric field leads to a higher harmonic yield and the production of two harmonic plateaus, although it is the first plateau that contributes to high conversion efficiency due to its high harmonic yield.

The results in Figure 8 show a graph of various static electric field values versus harmonic order. Here, the first and second harmonic plateaus and their respective harmonic cutoff points have been shown. From the graph, it can be clearly seen that as the static electric field is gradually increased, harmonic order also increases. The presence of static electric field influences the possibility of the returning electron to its parent ion leading to a recombination and subsequent emission of high order harmonics.

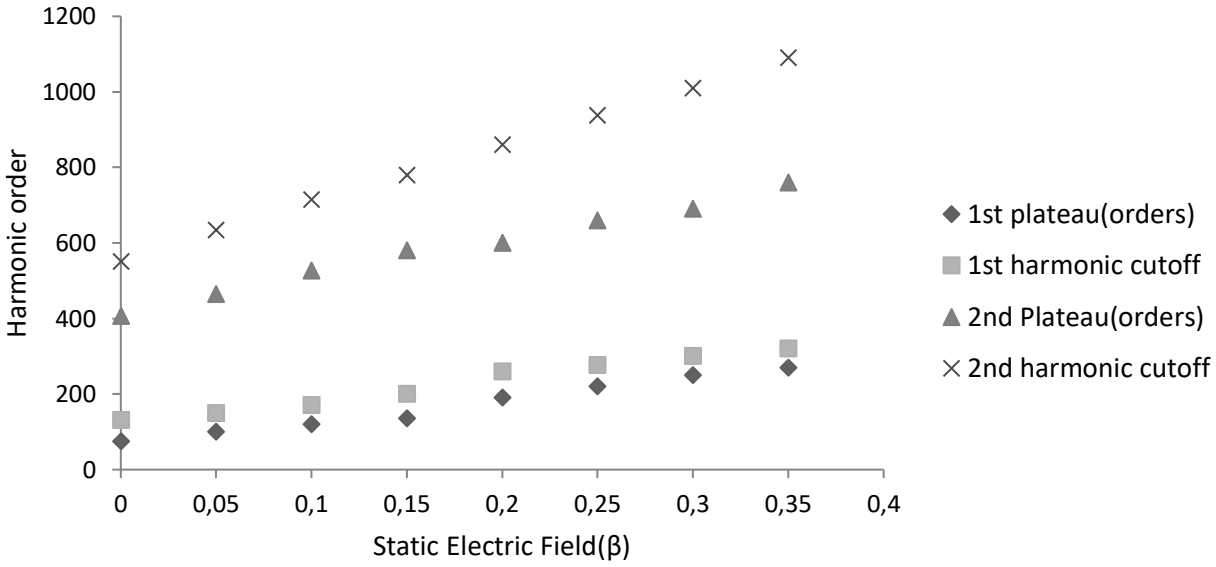

Figure 8. Graph of harmonic order against static electric field

4. Conclusion

Various factors that influence harmonic conversion efficiency have been studied. High harmonic conversion efficiency is achieved when the harmonic plateau is broadened and the cutoff point is extended. The results have shown that optimal harmonic conversion efficiency can be achieved with a combination of the following; a wavelength of 800nm for the fundamental pulse with an intensity of $4.0 \times 10^{14} W/cm^2$, 1600nm control pulse with an intensity of $3.6 \times 10^{14} W/cm^2$, polarization angle of 0.1π, inhomogeneity parameters of value 0.0010 and a static electric field value of 0.1. When these parameters are used simultaneously, we are able to obtain an extended harmonic cutoff to the 600^{th} order with few modulation structures, which is likely to lead to a favorite attosecond pulse.

Acknowledgements

We thank the Karatina University for providing the necessary facilities and resources to conduct my research.

Conflict of interest

The authors declare that there is no conflict of interest.

References

Abbing, S., Campi, F., Zeltsi, A., Smorenburg, P., & Kraus, P. M. (2021). Divergence and efficiency optimization in polarization-controlled two-color high-harmonic generation. *Scientific Reports*, *11*(1). https://doi.org/10.1038/s41598-021-03657-2

Bionta, M. R., Haddad, E., Leblanc, A., Gruson, V., Lassonde, P., Ibrahim, H., … François Légaré. (2021). Tracking ultrafast solid-state dynamics using high harmonic spectroscopy. *Physical Review Research*, *3*(2).

https://doi.org/10.1103/physrevresearch.3.023250

Boltaev, G. S., Iqbal, M., Abbasi, N. A., Kim, V. V., Ganeev, R. A., & Alnaser, A. S. (2021). Enhanced XUV harmonics generation from diatomic gases using two orthogonally polarized laser fields. *Scientific Reports*, *11*(1). https://doi.org/10.1038/s41598-021-85114-8

Burnett, K., & Rae, S. C. (1993). Calculations of high-order-harmonic generation in the strongly ionizing regime. *Physical Review A*, *48*(3), 2490–2493. https://doi.org/10.1103/physreva.48.2490

Chevreuil, P.-A. ., Brunner, F., Hrisafov, S., Pupeikis, J., Phillips, C. R., Keller, U., & Gallmann, L. (2021). Water-window high harmonic generation with 0.8-µm and 2.2-µm OPCPAs at 100 kHz. *Optics Express*, *29*(21), 32996. https://doi.org/10.1364/oe.440273

Ciappina, M. F., Jose Antonio Pérez-Hernández, Landsman, A. S., Okell, W. A., Sergey Zherebtsov, Förg, B., … Roso, L. (2017). Attosecond physics at the nanoscale. *Reports on Progress in Physics*, *80*(5), 054401–054401. https://doi.org/10.1088/1361-6633/aa574e

Constant, E., Nandi, S., Picot, C., Prost, E., S. Palakkal, F. Lépine, & V. Loriot. (2025). High order harmonic generation-based attosecond light sources and applications to quantum phenomena. *APL Photonics*, *10*(1). https://doi.org/10.1063/5.0235171

Davino, M., Summers, A., Saule, T., Tross, J., McManus, E., Davis, B., & Trallero-Herrero, C. (2021). Higher-order harmonic generation and strong field ionization with Bessel–Gauss beams in a thin jet geometry. *Journal of the Optical Society of America B*, *38*(7), 2194–2194. https://doi.org/10.1364/josab.420073

Feit, M. D., Fleck, J. A., & Steiger, A. (1982). Solution of the Schrödinger equation by a spectral method. *Journal of Computational Physics*, *47*(3), 412–433. https://doi.org/10.1016/0021-9991(82)90091-2

Feng, L., Yuan, M., & Chu, T. (2013). Attosecond x-ray source generation from two-color polarized gating plasmonic field enhancement. *Physics of Plasmas*, *20*(12), 122307–122307. https://doi.org/10.1063/1.4848757

Ganeev, R. A. (2022). High-order harmonic generation in laser-induced low-density plasma: past and recent achievements. *Applied Physics B*, *129*(1). https://doi.org/10.1007/s00340-022-07960-2

Gao, J., Wu, J., Lou, Z., Yang, F., Qian, J., Peng, Y., … Li, R. (2022). High-order harmonic generation in an x-ray range from laser-induced multivalent ions of noble gas. *Optica*, *9*(9), 1003–1003. https://doi.org/10.1364/optica.456481

Iqbal, M., Boltaev, G. S., Abbasi, N., Ganeev, R. A., & Alnaser, A. S. (2022). Spatial and spectral variations of high-order harmonics generated in noble gases. *Journal of Physics B: Atomic, Molecular and Optical Physics*, *55*(10), 105601. https://doi.org/10.1088/1361-6455/ac69c1

Kanega, M., Ikeda, T. N., & Sato, M. (2021). Linear and nonlinear optical responses in Kitaev spin liquids. *Physical Review Research*, *3*(3). https://doi.org/10.1103/physrevresearch.3.l032024

Kim, S., Jin, J., Kim, Y.-J., Park, I.-Y., Kim, Y., & Kim, S.-W. (2008). High-harmonic

generation by resonant plasmon field enhancement. *Nature*, *453*(7196), 757–760. https://doi.org/10.1038/nature07012

Koushki, A. M., R. Sadighi-Bonabi, M. Mohsen-Nia, & Irani, E. (2018). The control of electron quantum trajectories on the high-order harmonic generation of CO and N2 molecules in the presence of a low frequency field. *The Journal of Chemical Physics*, *148*(14). https://doi.org/10.1063/1.5018819

Koushki, A. M., & Sarikhani, S. (2020). High-order harmonic generation from CH4 and CD4 molecules in the presence of a static electric field. *Chemical Physics*, *541*, 111020. https://doi.org/10.1016/j.chemphys.2020.111020

Krause, J. L., Schafer, K. J., & Kulander, K. C. (1992). Calculation of photoemission from atoms subject to intense laser fields. *Physical Review A*, *45*(7), 4998–5010. https://doi.org/10.1103/physreva.45.4998

Krausz, F., & Ivanov, M. (2009). Attosecond physics. *Reviews of Modern Physics*, *81*(1), 163–234. https://doi.org/10.1103/revmodphys.81.163

Li, L., Lan, P., Zhu, X., & Lu, P. (2021). Huygens-Fresnel Picture for High Harmonic Generation in Solids. *Physical Review Letters (Print)*, *127*(22). https://doi.org/10.1103/physrevlett.127.223201

Li, X., Han, J., Liu, L., Wang, X., Wang, G., & Jin, C. (2024). Shaping extreme-ultraviolet attosecond pulses by tuning the minimum in high-order harmonic generation with two gas jets. *Physical Review. A/Physical Review, A*, *109*(2). https://doi.org/10.1103/physreva.109.023103

Neufeld, O., Zahra Nourbakhsh, Tancogne-Dejean, N., & Rubio, A. (2022). Ab Initio Cluster Approach for High Harmonic Generation in Liquids. *Journal of Chemical Theory and Computation*, *18*(7), 4117–4126. https://doi.org/10.1021/acs.jctc.2c00235

Njoroge, S. M., Yuan, H., Dickson, K., Zhang, Q., & Lan, P. (2019). Control of the polarization direction of isolated attosecond pulses using inhomogeneous two-color fields. *Scientific Reports*, *9*(1). https://doi.org/10.1038/s41598-019-54984-4

Njoroge, S., & Kinyua, D. (2024). High-order harmonic generation in a doped semiconductor by inhomogeneous laser field. In *Applied physics B, Lasers and optics*.

Park, J., Subramani, A., Kim, S., & Ciappina, M. F. (2021). Recent trends in high-order harmonic generation in solids. *Advances in Physics: X*, *7*(1). https://doi.org/10.1080/23746149.2021.2003244

Pérez-Hernández, J. A., Ciappina, M. F., Maciej Lewenstein, Roso, L., & A. Zaïr. (2013). Beyond CarbonK-Edge Harmonic Emission Using a Spatial and Temporal Synthesized Laser Field. *Physical Review Letters*, *110*(5). https://doi.org/10.1103/physrevlett.110.053001

Popmintchev, T., Chen, M.-C., Dimitar Popmintchev, Arpin, P., Brown, S., Skirmantas Alisauskas, … Kapteyn, H. C. (2012). Bright Coherent Ultrahigh Harmonics in the keV X-ray Regime from Mid-Infrared Femtosecond Lasers. *Science*, *336*(6086), 1287–1291. https://doi.org/10.1126/science.1218497

Rae, S. C., & Burnett, K. (1993). Calculations of high-order-harmonic generation in the

strongly ionizing regime. *Physical Review A*, *48*(3), 2490–2493. https://doi.org/10.1103/physreva.48.2490

Ren, S., Chen, D., Wang, S., Chen, Y., Hu, R., Qu, J., & Liu, L. (2024). Plasmon-Enhanced Circular Polarization High-Harmonic Generation from Silicon. *Advanced Optical Materials*, *12*(31). https://doi.org/10.1002/adom.202401478

Ren, X., Li, J., Yin, Y., Zhao, K., Chew, A., Wang, Y., … Chang, Z. (2017). Attosecond light sources in the water window. *Journal of Optics*, *20*(2), 023001–023001. https://doi.org/10.1088/2040-8986/aaa394

Salmeh, F., & Mohebbi, M. (2023). Generation of a single attosecond pulse by gaseous atoms in a conical plasmonic nanostructure using a radially polarized laser beam. *Optics & Laser Technology*, *170*, 110319. https://doi.org/10.1016/j.optlastec.2023.110319

Silaev, A. A., Romanov, A. A., & Vvedenskii, N. V. (2022). High Harmonic Generation from Oriented Asymmetric Molecules in the Presence of Static Electric Field. *Journal of Physics Conference Series*, *2249*(1), 012004–012004. https://doi.org/10.1088/1742-6596/2249/1/012004

Vincenti, H., S. Monchocé, S. Kahaly, G. Bonnaud, Martin, P., & F. Quéré. (2014). Optical properties of relativistic plasma mirrors. *Nature Communications*, *5*(1). https://doi.org/10.1038/ncomms4403

Wang, B., Li, X., & Fu, P. (1999). Effect of a Static Electric Field on High-Harmonic Generation in a Polarized Laser Field. *Chinese Physics Letters*, *16*(10), 723–725. https://doi.org/10.1088/0256-307x/16/10/008

Wang, X., Xiao, F., Wang, J., Wang, L., Zhang, B., Liu, J., … Zhao, Z. (2024). Ultrashort isolated attosecond pulses generation with 750 nm free-CEP near-infrared pulses. *Ultrafast Science*, *4*. https://doi.org/10.34133/ultrafastscience.0080

Weissenbilder, R., Carlström, S., Rego, L., Guo, C., Heyl, C. M., Smorenburg, P., … L'Huillier, A. (2022). How to optimize high-order harmonic generation in gases. *Nature Reviews Physics*, *4*(11), 713–722. https://doi.org/10.1038/s42254-022-00522-7

Xiaohong, S., Yang, S., Wang, G., Lin, J., Wang, L., & Meier, T. (2023). Control of the electron dynamics in solid-state high harmonic generation on ultrafast time scales by a polarization-skewed laser pulse. *Optics Express*, *22;31(12):18862–2*.

Yu, R., Yu, E., & V, S. (2021). Attosecond electromagnetic pulses: generation, measurement, and application. Attosecond metrology and spectroscopy. *Physics-Uspekhi [Internet*, *1;66(04):360–80*. Retrieved from https://www.ufn.ru/ufn2023/ufn2023_4/ufn234b.pdf

Yu, W., Liang, H., Geng, L., & Peng, L.-Y. (2023). Dynamical analysis of attosecond molecular modes. Physical Review. A/Physical Review, A, 107(1). https://doi.org/10.1103/physreva.107.013101

Yuan, H., He, L., Wang, F., Wang, B., Liu, W., & Hong, Z. (2017). Generation of isolated attosecond pulses in a multi-cycle inhomogeneous two-color field without CEP stabilization. *Optical and Quantum Electronics*, *49*(6). https://doi.org/10.1007/s11082-017-1048-x

Yue, L., & Gaarde, M. B. (2021). Expanded view of electron-hole recollisions in solid-state high-order harmonic generation: Full-Brillouin-zone tunneling and imperfect recollisions. *Physical Review*, *103*(6). https://doi.org/10.1103/physreva.103.063105

Yue, L., Yue, L., Gaarde, M. B., & Gaarde, M. B. (2022). Introduction to theory of high-harmonic generation in solids: tutorial. *JOSA B*, *39*(2), 535–555. https://doi.org/10.1364/JOSAB.448602

Zhang, G.-T., Bai, T.-T., & Zhang, M.-G. (2012). Generation of an isolated sub-30 attosecond pulse in a two-color laser field and a static electric field. *Chinese Physics B*, *21*(5), 054214. https://doi.org/10.1088/1674-1056/21/5/054214